Enhanced magnetoresistance by monoatomic roughness in epitaxial Fe/MgO/Fe tunnel junctions

A. Duluard, C. Bellouard,[*] Y. Lu, M. Hehn, D. Lacour, F. Montaigne, G. Lengaigne, and S. Andrieu

Institut Jean Lamour, UMR 7198, CNRS-Université de Lorraine, Boîte Postale 239, 54506 Vandoeuvre, France

F. Bonell

CIN2 (CSIC-ICN) Catalan Institute of Nanotechnology, Physics and Engineering of Nanodevices, Campus Universidad Autónoma de Barcelona, E-08193 Bellaterra, Barcelona, Spain

C. Tiusan[†]

Department of Physics and Chemistry, Center for Superconductivity, Spintronics and Surface Science, Technical University of Cluj-Napoca, Cluj-Napoca, Romania
and Institut Jean Lamour, UMR 7198, CNRS-Université de Lorraine, Boîte Postale 239, 54506 Vandoeuvre, France

Interfacial effects on spin and symmetry filtering in single-crystal Fe(001)/MgO/Fe magnetic tunnel junctions are investigated with the insertion of a Fe monoatomic step at the bottom MgO interface. After annealing, the atomically flat bottom electrode is covered by a fractional part of a Fe monoatomic layer resulting in two-dimensional Fe islands that are separated for low coverages and percolated above around half a monolayer. The magnetotransport properties of the junctions are studied as a function of this Fe sublayer coverage that is varied from 0 to 1 monolayer. Surprisingly, the magnetoresistance ratio exhibits a maximum for a coverage around half a monolayer. Tunneling spectroscopy experiments performed at low temperature allow relating this result to the decrease of the contribution of the interfacial resonance state to the conductance of the junction.

I. INTRODUCTION

A huge tunnel magnetoresistance (TMR) ratio, above 1000%, has been predicted in single-crystalline Fe/MgO/Fe(001) magnetic tunnel junctions (MTJs) [1,2]. This very peculiar property is directly related to the electronic band structure of bulk iron along the [001] direction (Δ direction) combined with the symmetry-dependent tunnel decay rate of the MgO barrier. For thick barriers, in the so-called asymptotic regime, the Fe electrode should behave like a half-metal. As a matter of fact, numerous experimental studies have been carried out on single-crystal MTJs [3], but all of them led to limited TMR values, between 180% and 250% at room temperature and between 300% and 475% at low temperature as reported in the literature [4–10]. Moreover, quite similar results have been obtained with textured junctions, which are, however, intuitively expected to be less effective [11]. On the other hand, much higher TMRs have been reached with textured FeCoB electrodes grown by sputtering [12]. Despite significant TMR ratio improvement, the relation between high crystallinity and transport properties is then far from being obvious in this system. Concerning the epitaxial Fe(001)/MgO MTJs, the impact of chemical and structural defects has been experimentally checked. It has been shown that volume defects in the barrier as misfit dislocations are detrimental for TMR [13–16]. Surprisingly, controlled contamination of the interface with carbon [17,18], or oxygen has been found to have small impact on TMR values (at zero voltage) [19,20]. From a theoretical point of view, the difficulty is then to quantify the effect of these

defects on the electronic band structure. In the case of carbon contamination at the interface, good agreements have been observed between experimental features and *ab initio* calculation [18]. Historically, carbon contamination of bottom Fe(001)/MgO interface in MTJs allowed the observation of the signature of the Fe surface state in magnetotransport measurements with MTJs in the asymptotic regime [17]. This surface state lies in the minority band, and the enhancement of its Δ1 spectral density with the presence of carbon leads to a sign reversal of the TMR for a specific bias which activates the conduction channel associated to this surface state. More recently, this reversal has been observed even with an undoped Fe/MgO interface in the thin barrier regime [21]. Here, the tunneling propagation of Bloch states with $k_{//} \neq 0$ and various symmetries is allowed across the MgO(001) barrier and then the complete activation of the surface state is achieved (all its spectral components contribute to tunneling). Moreover, the surface state is indeed observed in the case of a very flat interface, and is completely missing in the case of a rough interface [21]. In the case of the flat interface, in the asymptotic regime corresponding to thick MgO barriers, this surface state has less effect on tunneling than in the case of a thin barrier because of a symmetry-dependent attenuation rate across the (001)MgO barrier [21]. Consequently, no reversal of the TMR is observed, the only effect being a steeper decrease of the TMR with the applied voltage. The detrimental effect on the TMR of a surface state lying in the minority band close to the Fermi level has been clearly shown for the $Fe_xCo_{1−x}$/MgO junction where the properties of the surface state can be tuned with the alloy concentration [22]. On the other hand, one can argue that the interface state at the Fe(001)/MgO interface has a negative spin polarization which competes with the positive bulk polarization of Fe and therefore can have a negative effect on the total

*christine.bellouard@univ-lorraine.fr
†coriolan.tiusan@phys.utcluj.ro

effective polarization of the Fe electrode in the single-crystal Fe(001)/MgO MTJs. The interface states which contain Δ_1 symmetry states favor a conduction channel in antiparallel configuration which should be forbidden by bulk states. In that case, a possible detrimental effect of this interface state on the TMR amplitude at low bias is suspected but still remains unclear. Therefore, a possible way for the TMR enhancement would be the quenching of the Fe interface state or its shift in energy above or below the Fermi level. Theoretically, it has been proposed that an interfacial Ag monolayer would suppress tunneling through the interfacial state, and then increase the TMR [23].

In the present study, we propose to affect or quench the interface state by creating some controlled roughness at the Fe/MgO interface. This goal can be achieved by growing less than an atomic Fe plane on top of the flat Fe electrode, leading to a topological modulation of the bottom Fe(001) surface at the interface with the MgO barrier. Using an *in situ* shutter, a Fe wedge ranging from 0 to 1 monolayer (ML) is deposited. It results in a coverage with Fe islands of varying size, which modulate the interface roughness in a reproducible and controlled manner. To investigate the quality of the tunnel barrier grown on different Fe surface qualities, the reflection high-energy electron diffraction (RHEED) patterns have been recorded during Fe and MgO growth. The evolution of reflected intensity, surface parameter, and linewidth during MgO growth, on flat or decorated surfaces, are compared. The room temperature magnetotransport properties of the junctions in the asymptotic regime (thick MgO barrier) were thus studied by varying the coverage (in the submonolayer range) of this last Fe atomic layer just below MgO. The impact of this topological surface modulation on the surface state was thus studied through tunneling spectroscopy measurements. Surprisingly, the TMR ratio exhibits a maximum for a covering ratio of about 0.5 ML. Tunneling spectroscopy experiments performed on patterned MTJs at low temperature allow to explain this result in terms of surface state properties. Our results show that the TMR enhancement is related to the IRS (interfacial resonance state) quenching on the border of the Fe terraces.

II. EXPERIMENTAL DETAILS

The MTJs are grown by molecular beam epitaxy (MBE) controlled by *in situ* reflection high-energy electron diffraction. Previous to deposition, the (001)MgO substrate has been outgassed at 650 °C for 30 min, and covered by a 10-nm MgO trapping layer, which prevents carbon diffusion in the stack during subsequent annealing [24]. Fe has been evaporated either from a Knudsen cell (growth study) or with electron bombardment (transport study). The whole stack is MgO(10 nm)/Fe(60 nm)/Fe(from 0 to 1 ML)/MgO(10 or 11 ML)/Fe(13 nm)/Co(30 nm)/Au(10 nm). The deposited barrier thicknesses have been determined with oscillations of RHEED intensity. After deposition at room temperature, the 60-nm-thick Fe layer has been annealed at 500 °C for 30 min in order to flatten its surface. The 0–1 ML Fe wedge is then deposited at a substrate temperature of 100 °C thanks to an *in situ* moving shutter. The Fe covering of the flat Fe layer modulates the size of the Fe islands which results in a controlled interfacial roughness. The growth of the

single-crystalline MgO barrier is then performed at a substrate temperature of 100 °C with monitoring by RHEED intensity oscillations. The *in situ* shutter is used again in order to get MTJ systems with two different barrier thicknesses on the same wafer. Then, the second Fe/Co electrode is deposited without any annealing, in order to avoid any rearrangement at the bottom Fe/MgO interface. Finally the stack is covered by a 10-nm Au capping layer. Electrical characterization was completed using a two-probes method on 10–40 μm square MTJs, patterned by a combined UV lithography/ion etching process. Each set of results presented as a function of the Fe covering rate is obtained with junctions aligned in the wedge direction and with the same size. Low-temperature measurements are performed in a Physical Properties Measurement System (PPMS from Quantum Design) supplied with a specific rod (lab-made).

III. RESULTS

A. Growth study

Figure 1(a) shows a RHEED pattern of a Fe (100) flat surface in the [10] azimuth and the profile used for the growth study. The first-order diffraction lines of the profile are then fitted by Lorentz laws [Fig. 1(b)], and three parameters are extracted: the intensity, the full width at half maximum, and the relative surface lattice spacing.

Previous to the MgO barrier growth study, we focus on the Fe growth on Fe, which provides information on the initial flat or atomically rough surface. An example of the variation of the intensity, linewidth, and in-plane surface lattice spacing as a function of Fe coverage is plotted in Fig. 2. Oscillations of all parameters are observed for the first deposited layers, with a maximum (respectively, minimum) value of the intensity (respectively, linewidth) reached for full filled layers [Figs. 2(a) and 2(b)]. Oscillations of lattice spacing in homoepitaxy have already been observed in the case of Fe, V, or Nb [25]. They can been explained by angular dispersion of the incident beam [26], or size effect (the lattice
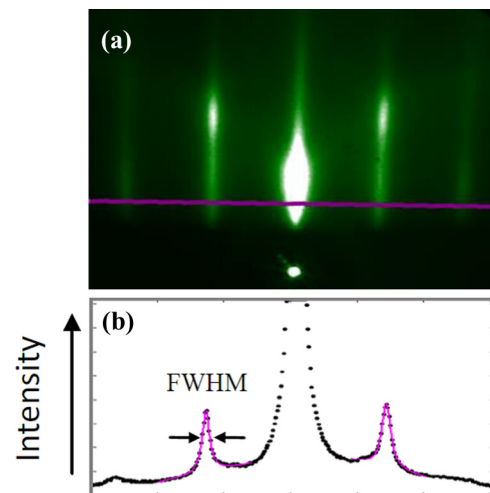

FIG. 1. (Color online) (a) RHEED pattern in the [10] azimuth of a (001)Fe surface; (b) intensity profile (points) and fit (straight line) with Lorentzian laws.
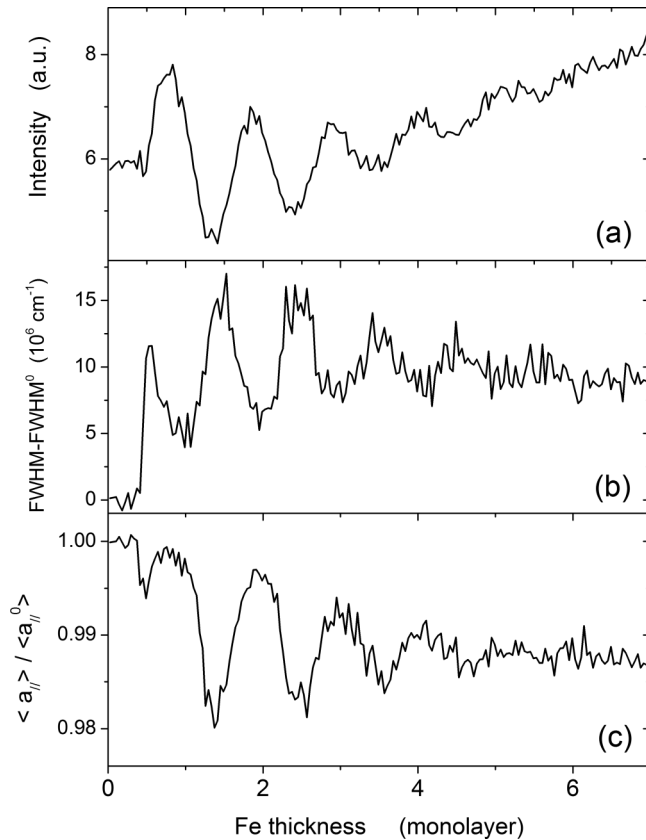
FIG. 2. Example of evolution of growth parameters extracted from the analysis of RHEED profiles with deposited thickness during growth of Fe on flat Fe(100): Intensity (a); increase of the full width at half maximum with respect to the value of the flat surface (b); relative in-plane lattice spacing (c).

parameter of a nanoisland is not similar to the bulk) and can be enhanced by surface contamination (carbon or/and oxygen contamination may occur on Fe, V, or Nb buffer layers as sometimes observed by Auger spectroscopy) [27]. In the present study, no surface contamination was evidenced but even a low surface contamination that is difficult to detect may affect the nucleation density, and then the island's size. In this example, we observed a decrease of the lattice spacing of 0.5% for a Fe coverage of 0.5 ML. This may vary from one experiment to another, but the effect remains between 0% and 1%.

Previous studies based on an analysis of RHEED diffraction pattern have shown that it is possible to evaluate the nucleation density during a two-dimensional growth [25,28]. It has been experimentally verified that the full width at half maximum of the RHEED streaks provides an estimation of the nucleation density N when the experiment is performed in anti-Bragg geometry [29]. Following this procedure, a systematic study has been performed as a function of the substrate temperature for a Fe coverage $\theta = 0.5$ ML. Based on several experiments performed on different samples, the nucleation density $N = [\frac{\text{FWHM}(\theta=0.5) - \text{FWHM}(\theta=0)}{4 \pi}]^2$ was estimated around $(1.2 \pm 0.4) \, 10^{12} \, \text{cm}^{-2}$. This value is in agreement with previous results presented in Ref. [27]. This global agreement with other experiments allows us to evaluate the average

distance between islands for a substrate temperature around $100 \, °\text{C}$, $L = \frac{1}{\sqrt{N}} \approx (9 \pm 2)$ nm. The average island size a was also estimated using the relation between the coverage and the surface occupied by an island (assumed to be squared) as $\theta \cong Na^2$. We thus obtained the average island size for $\theta = 0.5$ ML as $a = L \sqrt{\theta} = 6$ nm.

In a next step, the growth of MgO has been studied upon a flat Fe surface or upon Fe islands (Fe 0.5 ML). This study has been performed in the $[10]_{\text{Fe}}$ azimuth, with a substrate temperature of $100 \, °\text{C}$, and a constant MgO growth rate close to $0.1 \, \text{Å s}^{-1}$. From the recorded RHEED patterns, intensity profiles are extracted at the same location of the pattern in both studies [25]. The evolution of these parameters during MgO growth on flat Fe is presented in Figs. 3(a)–3(d). This growth is known to be layer by layer with a lattice spacing mismatch: $a_{\text{MgO}}/\sqrt{2} \, a_{\text{Fe}} = 1.036$. In that case, as usually observed [30], two growth regimes can be distinguished, as indicated by the vertical arrow. For a deposited MgO thickness less than 5 ML (as evaluated by the intensity oscillations), the growth is so-called pseudomorphic, that is, the deposited layers are strained by the buffer and the lattice parameter is almost constant [Fig. 3(b)]. Above this critical thickness, the lattice parameter relaxes towards the MgO bulk value (relative value = 1.036) with the occurrence of dislocations. One can notice the phase relationship of the oscillations of the three parameters, in perfect agreement with theory [25]. Figures 3(c) and 3(d) present the same parameters in the case of MgO growth upon 0.5 Fe ML. Again, the two regimes can be clearly distinguished, as shown by the vertical arrow. In fact, after the deposition of 1.5–2 ML of MgO, as indicated by the dashed lines and black points, the behavior of the three parameters is very similar in both cases: for instance, the full width at half maximum (FWHM) presents a minimum at the crossover between the two regimes and reaches the same maximum value (≈ 15 a.u.) after the deposition of about 14 ML. However, the main discrepancies occur at the very first stage of the deposition (between 0 and 2 ML) for the three parameters. In particular, the relative lattice spacing increases more rapidly in the case of islands (about 2%) than in the case of flat Fe (roughly 1%) as indicated by the black point. In fact, one has to take into account the lower surface lattice parameter of 0.5 Fe ML with respect to that of flat Fe [0.5%, from Fig. 2(c)], as noted above. The scale on the right side of the plot is calibrated with respect to the parameter of flat Fe. In that case, the parameter reached after relaxation is close to the value reached in the case of a flat surface. As a conclusion, the introduction of a half Fe monolayer before the growth of MgO modifies the very first stage of the growth (0–2 ML) but has no clear impact on the MgO barrier plastic relaxation, as can be observed within the RHEED coherence length scale. From this detailed structural analysis, in the following, we will thus assume that there are no significant differences between the volume properties of MgO barriers deposited on flat Fe surface or Fe islands.

B. Transport measurements

Based on the results of the *in situ* structural analysis, MTJ complete stacks with topologically modulated bottom Fe(001)/MgO interfaces have been grown, patterned, and submitted to magnetotransport analysis. MTJs with similar
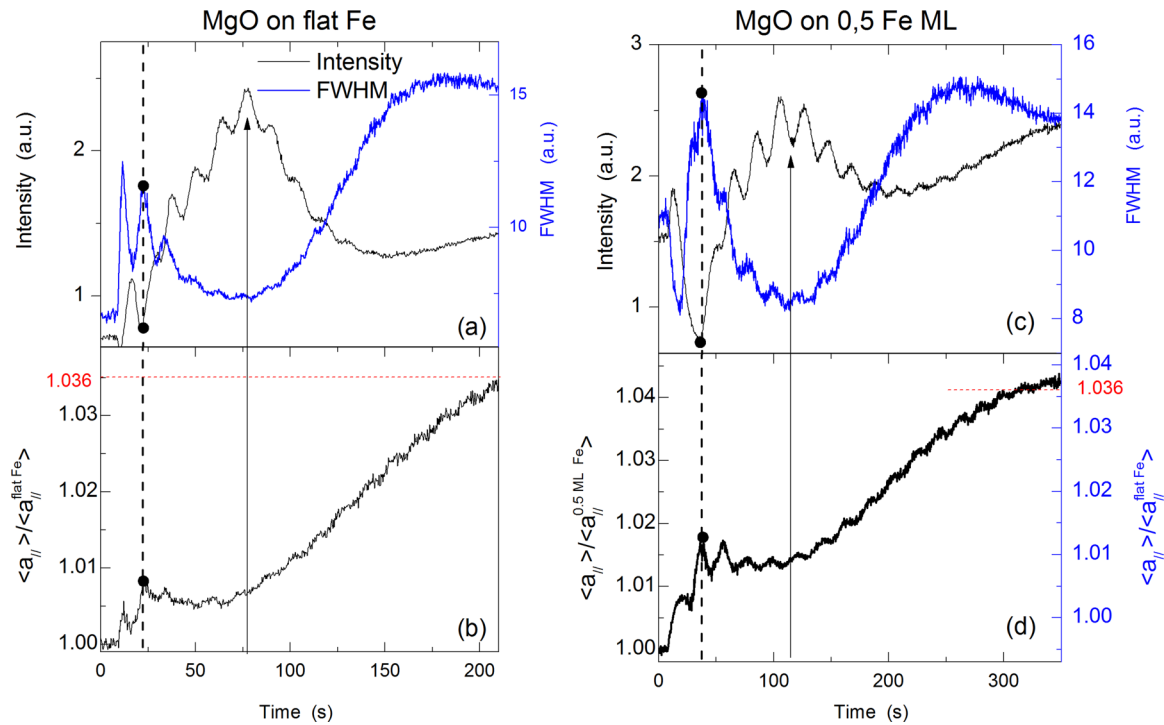
FIG. 3. (Color online) Comparison of growth parameters extracted from the analysis of RHEED profiles (intensity, FWHM) and relative surface lattice spacing $a_{//}$ of MgO deposited on flat Fe (a,b) with that on Fe islands (c,d), respectively.

interfaces but with two different MgO barrier thicknesses have been analyzed to have access to attenuation features of the tunneling transport channels.

Results of room temperature transport measurements are plotted in Figs. 4(a)–4(c) as a function of Fe coverage for both MgO thicknesses (10 and 11 ML). The $R(H)$ loops (not shown here) present steep reversals, and antiparallel states (AP) are well defined by wide plateaus. The TMR values [Fig. 4(a)] measured for the reference junctions (flat Fe buffer) are about 100%. This TMR value is well below the 180% usually obtained at room temperature in single-crystalline Fe/MgO/Fe MTJs [18]. Indeed, we recall that the hard electrode of the MTJ has not been annealed (as for high TMR ratio junctions) to avoid any structural rearrangements at the bottom interface.

Figure 4(a) shows that the introduction of a small amount of Fe at the bottom interface leads to a strong increase of the TMR for both MgO barrier thicknesses. It reaches a maximum of 122% around the half covering for a barrier thickness of 10 ML. Then, the TMR decreases towards its reference value as the Fe covering increases from 0.5 to 1 ML. We point out that this maximum TMR value measured at half coverage, that is to say, for a maximum density of Fe steps or defects at the Fe(001)/MgO interface, is absolutely unexpected. To get a better understanding of the TMR variation with the interfacial Fe coverage ratio, we analyze the parallel (P) and antiparallel resistances (R_P and R_{AP}) of the MTJs. Figures 4(b) and 4(c) present the evolution of R_P and R_{AP} referred to the flat surface. In both cases, a maximum is observed at half coverage, with a higher value for the AP resistance, which explains the increase of TMR. The increase of resistance with the introduction of Fe islands indicates that a conduction channel is reduced with

the presence of Fe steps, and the effect is stronger in the AP configuration. The increase of TMR with Fe covering cannot be associated to the presence of a contamination, as the initial reference values of resistances are recovered after a full layer deposition. Therefore, the maximum TMR at half covering must then be correlated to the maximum density of steps.

Further insight on those results can be extracted from tunneling spectroscopy experiments. Figures 4(d)–4(f) gather and correlate the bias dependence of the TMR $= \frac{R_{AP}-R_P}{R_P}$, conductances $G_x = \frac{dI_x}{dV}$, and the absolute value of the derivative of the antiparallel conductance measured at 5 K for 11 ML MgO thickness, and three Fe covering ratios, 0, 0.2, and 0.6 Fe ML. It should be noted that the transport properties presented here are obtained on different MTJs patterned on the same sample, with the same lithography process. Thus a quantitative comparison of the transport results obtained from one MTJ to the other is pertinent.

For negative voltage, electrons are injected towards the bottom electrode. Therefore, the measured tunnel current convolutes the occupied states of the top electrode, lying near E_F with the electronic structure features of the unoccupied states in the bottom electrode. We firstly comment common features of the three interfaces. The voltage dependence of the TMR [Fig. 4(d)] presents a very asymmetric shape, with a strong decrease of the TMR for negative voltages above -0.2 V for the three interfaces. As usual with Fe/MgO junctions, the voltage dependence of the TMR has to be correlated to the AP conductance. This conductance indeed exhibits a strong increase for negative voltage above -0.2 V [Fig. 4(e)] whereas the voltage dependence of the parallel conductance is weaker [Fig. 4(e)]. This asymmetry of G_{AP} is
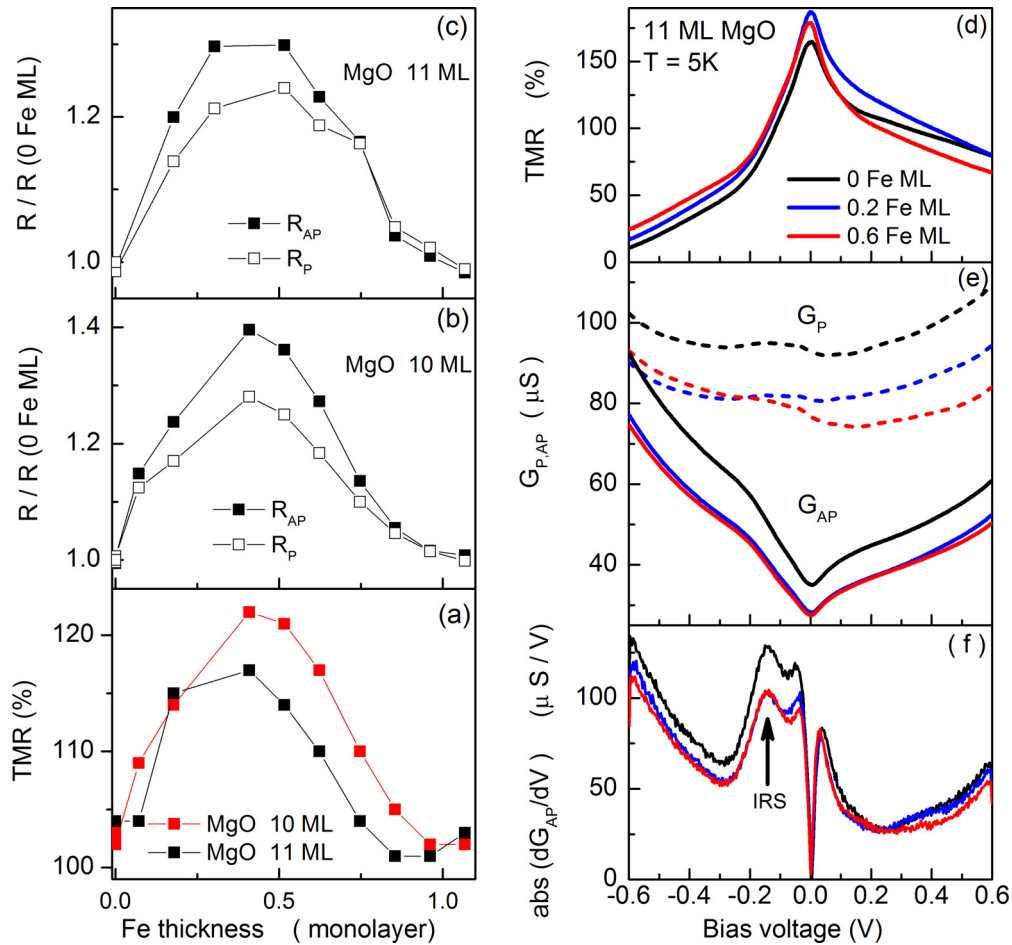
FIG. 4. (Color online) Effect of Fe coverage measured at $T = 300$ K on (a) the TMR ratio; the AP and P resistance normalized with respect to flat Fe surface for two barrier thicknesses 10 ML (b) and 11 ML (c). Bias dependence, measured at 5 K, for the 11 ML MgO barrier and three Fe covering ratios (0, 0.2, 0.6 ML) of (d) TMR; (e) parallel and antiparallel differential conductance (G_P G_{AP}); (f) absolute value of the derivative of G_{AP} (V).

clearly shown in Fig. 4(f) which presents the absolute value of its derivative. In Fig. 4(f), three peaks are observed: Two symmetric ones are located at ± 0.037 V attributed to magnon excitations [18]; the stronger one located only at -0.14 V reveals the asymmetry of the interfacial electronic structure. It has been previously attributed to the interfacial resonance state surviving in MTJ stacks with a high-quality bottom interface [31]. Previous studies have shown that it can be tuned by interface quality [21] or chemical doping [18]. It is located in the minority band and arrives in the $\bar{\Gamma}$ point just above the Fermi level. This interface state then dominates the voltage dependence of the antiparallel conductance at negative voltage when it is activated for tunneling. It plays a major role in the case of low MgO thickness, as it is responsible for a reversal of the TMR [21]. We focus now on the differences between the three bottom Fe/MgO interfaces corresponding to different Fe underlayer coverage ratios. At 5 K, the TMRs of the junction with 0.2 or 0.6 Fe ML at the bottom interface are improved at low voltage, as observed at room temperature. Their asymmetrical shape is slightly corrected with respect to the reference junction (flat Fe/MgO interface) when disordering the bottom interface. Concerning the parallel conductance, two features can be pointed out

from the bias dependence plotted in Fig. 3(e): It is globally decreased in the -0.6, 0.6 V range in the presence of islands, and this decrease is steeper at positive voltage for the 0.6 Fe ML interface. Assuming that within the asymptotic tunneling regime (our case), the parallel conductance is dominated by majority spins with Δ_1 symmetry, any defect inducing a scattering of a pure Δ_1 state towards Bloch states with more attenuated symmetry will decrease the conductance. However, this effect would be bias independent. The steeper decrease at 0.6 Fe ML for positive voltage, when electrons flow from the occupied states of the bottom electrode to the top electrode, involves a more specific feature of the electronic structure on tunneling in the parallel MTJ magnetization configuration. As a contribution of the minority spin density is also present in G_P through the minority to minority channel, the decrease of G_P for positive voltage could be due to a decrease of the contribution of the occupied minority channel at the Fermi level of the bottom electrode. This point is in fact further supported by the analysis of G_{AP}. The main effect induced by the Fe islands is indeed observed for the AP conductance at negative voltage. The conductance is then dominated by the channel arising from majority spins of the top electrode flowing towards the minority states available above the Fermi

level of the bottom electrode. Figure 4(f) shows that the main difference between MTJ systems with topologically modulated bottom Fe/MgO interfaces is the attenuation of the IRS peak at -0.14 V. Moreover, an overall decrease of $|\frac{dG_{AP}}{dV}|$ in the presence of the decorated interface at negative voltage is observed whereas the curves are well superimposed at positive voltage, when electrons flow towards the upper interface. From this tunneling transport analysis we can conclude that, clearly, the presence of islands at the bottom interface has lowered the weight of the conduction mediated by the IRS. Because of the negative spin polarization of these states, it results in an improvement of the TMR ratio measured at low voltage. Interestingly, the present macroscopic study corroborates the results obtained in Ref. [32] on local electronic structure by scanning tunneling spectroscopy (vacuum interface). They found that the Fe(001)surface state is completely quenched along [100] and [110] monoatomic steps. Therefore, magnetotransport and tunneling spectroscopy experiments, performed on single-crystal Fe(001)/MgO/Fe MgO with topologically modulated bottom interfaces, demonstrate that the IRS quenching leads to an enhancement of the tunneling spin polarization and consequently, of TMR amplitude at zero bias.

IV. CONCLUSION

In conclusion, transport properties of single-crystal Fe(001)/MgO/Fe junctions have been investigated as a function of controlled structural defects inserted at the bottom interface. These defects consist of monoatomic Fe islands whose size is varied with covering ratio. Surprisingly, a maximum TMR is observed for a covering rate of 0.5 Fe ML, which means for a maximum density of steps. A spectroscopic analysis allows attributing this effect to a decrease of the channel conduction mediated by the interface resonance state. As this state is located in the minority band, near the Fermi level, it has a stronger impact on the antiparallel conductance than on the parallel one. This explains the TMR amplitude enhancement when the IRS is quenched. This result demonstrates that in single-crystal Fe(001)/MgO MTJs the relation between structural quality and TMR is counterintuitive, with a maximum disorder inducing a maximum TMR. Our results can be extrapolated to provide further understanding of mechanisms responsible for larger TMR ratios measured in sputtered MgO based textured MTJs. The quenching/absence of the surface state in these systems may contribute to their better TMR performance. Moreover, the present study corroborates a local investigation of the electronic structure by scanning tunneling microscopy in the case of vacuum interface which has shown that the interfacial resonance state is quenched along monoatomic Fe steps [32]. Interestingly, Bischoff *et al.* have shown that this surface state is shifted towards higher energy with decreasing island size. As a perspective study, decreasing the island's size would then be worth investigating as it should also increase the density of steps, particularly in the low barrier thickness regime where the surface state dominates the TMR behavior.

[1] W. H. Butler, X.-G. Zhang, T. C. Schulthess, and J. M. MacLaren, Phys. Rev. B **63**, 054416 (2001).

[2] J. Mathon and A. Umerski, Phys. Rev. B **63**, 220403(R) (2001).

[3] X. F. Han, S. S. Ali, and S. H. Liang, Sci. China: Phys., Mech. Astron. **56**, 29 (2013).

[4] S. Yuasa, T. Nagahama, A. Fukushima, Y. Suzuki, and K. Ando, Nat. Mater. **3**, 868 (2004).

[5] S. S. P. Parkin, C. Kaiser, A. Panchula, P. M. Rice, B. Hughes, M. Samant, and S.-H. Yang, Nat. Mater. **3**, 862 (2004).

[6] S. Yuasa, A. Fukushima, H. Kubota, Y. Suzuki, and K. Ando, Appl. Phys. Lett. **89**, 042505 (2006).

[7] C. Tiusan, M. Hehn, F. Montaigne, F. Greullet, S. Andrieu, and A. Schuhl, J. Phys.: Condens. Matter. **19**, 165201 (2007).

[8] Q. L. Ma, S. G. Wang, J. Zhang, Yan Wang, R. C. C. Ward, C. Wang, A. Kohn, X.-G. Zhang, and X. F. Han, Appl. Phys. Lett. **95**, 052506 (2009).

[9] J. M. Teixeira, J. Ventura, J. P. Araujo, J. B. Sousa, P. Wisniowski, and P. P. Freitas, Appl. Phys. Lett. **96**, 262506 (2010).

[10] K. Dumesnil and S. Andrieu, Epitaxial magnetic layers grown by MBE: Model systems to study the physics in nanomagnetism and spintronic, in *Molecular Beam Epitaxy: From Research to Mass Production*, edited by M. Henini (Elsevier, Amsterdam, 2012), Chap. 20.

[11] A. Duluard, B. Negulescu, C. Bellouard, M. Hehn, D. Lacour, Y. Lu, G. Lengaigne, F. Montaigne, S. Robert, S. Suire, and C. Tiusan, Appl. Phys. Lett. **100**, 072408 (2012).

[12] S. Ikeda, J. Hayakawa, Y. Ashizawa, Y. Lee, K. Miura, H. Hasegawa, M. Tsunoda, F. Matsukura, and H. Ohno, Appl. Phys. Lett. **93**, 082508 (2008).

[13] F. Bonell, S. Andrieu, F. Bertran, P. Lefevre, A. Taleb-Ibrahimi, E. Snoeck, C. Tiusan, and F. Montaigne, IEEE Trans. Magn. **45**, 3467 (2009).

[14] C. Wang, A. Kohn, S. G. Wang, L. Y. Chang, S.-Y. Choi, A. I. Kirkland, A. K. Petford-Long, and R. C. C. Ward, Phys. Rev. B **82**, 024428 (2010).

[15] F. Bonell, S. Andrieu, C. Tiusan, F. Montaigne, E. Snoeck, B. Belhadji, L. Calmels, F. Bertran, P. Le Fevre, and A. Taleb-Ibrahimi, Phys. Rev. B **82**, 092405 (2010).

[16] M. S. Gabor, C. Tiusan, T. Petrisor, Jr., T. Petrisor, M. Hehn, Y. Lu, and E. Snoeck, J. Magn. Magn. Mater. **347**, 79 (2013).

[17] C. Tiusan, M. Sicot, M. Hehn, C. Belouard, S. Andrieu, F. Montaigne, and A. Schuhl, Appl. Phys. Lett. **88**, 62512 (2006).

[18] Y. Lu, H.-X. Yang, C. Tiusan, M. Hehn, M. Chshiev, A. Duluard, B. Kierren, G. Lengaigne, D. Lacour, C. Bellouard, and F. Montaigne, Phys. Rev. B **86**, 184420 (2012).

[19] F. Bonell, S. Andrieu, A. M. Bataille, C. Tiusan, and G. Lengaigne, Phys. Rev. B **79**, 224405 (2009).

[20] P. J. Zermatten, F. Bonell, S. Andrieu, M. Chshiev, C. Tiusan, A. Schuhl, and G. Gaudin, Appl. Phys. Express **5**, 023001 (2012).

[21] R. B. Gangineni, C. Bellouard, A. Duluard, B. Negulescu, C. Baraduc, G. Gaudin, and C. Tiusan, Appl. Phys. Lett. **104**, 182402 (2014).

[22] F. Bonell, T. Hauet, S. Andrieu, F. Bertran, P. Le Fèvre, L. Calmels, A. Tejeda, F. Montaigne, B. Warot-Fonrose, B. Belhadji, A. Nicolaou, and A. Taleb-Ibrahimi, Phys. Rev. Lett. **108**, 176602 (2012).

[23] E. Y. Tsymbal, K. D. Belashchenko, J. P. Velev, S. S. Jaswal, M. van Schilgaarde, I. I. Oleynik, and D. A. Stewart, Prog. Mater. Sci. **52**, 401 (2006).

[24] M. Sicot, S. Andrieu, C. Tiusan, F. Bertran, and F. Montaigne, J. Appl. Phys. **99**, 301 (2006)

[25] P. Turban, L. Hennet, and S. Andrieu, Surf. Sci. **446**, 241 (2000).

[26] J. D. Fuhr and P. Müller, Phys. Rev. B **84**, 195429 (2011)

[27] P. Turban, F. Dulot, B. Kierren, and S. Andrieu, Appl. Surf. Sci. **177**, 282 (2001).

[28] P. Turban, P. Müller, L. Lapena, and S. Andrieu, Appl. Surf. Sci. **188**, 97 (2002).

[29] P. Müller, P. Turban, L. Lapena, and S. Andrieu, Surf. Sci. **488**, 52 (2001).

[30] J. L. Vassent, M. Dynna, A. Marty, B. Gilles, and G. Patrat, J. Appl. Phys. **80**, 5727 (1996).

[31] C. Tiusan, J. Faure-Vincent, C. Bellouard, M. Hehn, E. Jouguelet, and A. Schuhl, Phys. Rev. Lett. **93**, 106602 (2004).

[32] M. M. J. Bischoff, T. K. Yamada, C. M. Fang, R. A. de Groot, and H. van Kempen, Phys. Rev. B **68**, 045422 (2003).